Supplemental Figures and Tables

Caprin-1 binding to the critical stress granule protein G3BP1 is influenced by pH

Tim Schulte*[1], Marc D. Panas*[2], Xiao Han[1], Lucy Williams[2], Nancy Kedersha[3], Jonas Simon Fleck[1], Timothy J.C. Tan[2], Xaquin Castro Dopico[2], Anders Olsson[4], Ainhoa Moliner Morro[2], Leo Hanke[2], Johan Nilvebrant[5], Kim Anh Giang[5], Per-Åke Nygren[5], Paul Anderson[3], Adnane Achour#[1], Gerald M. McInerney#[2]

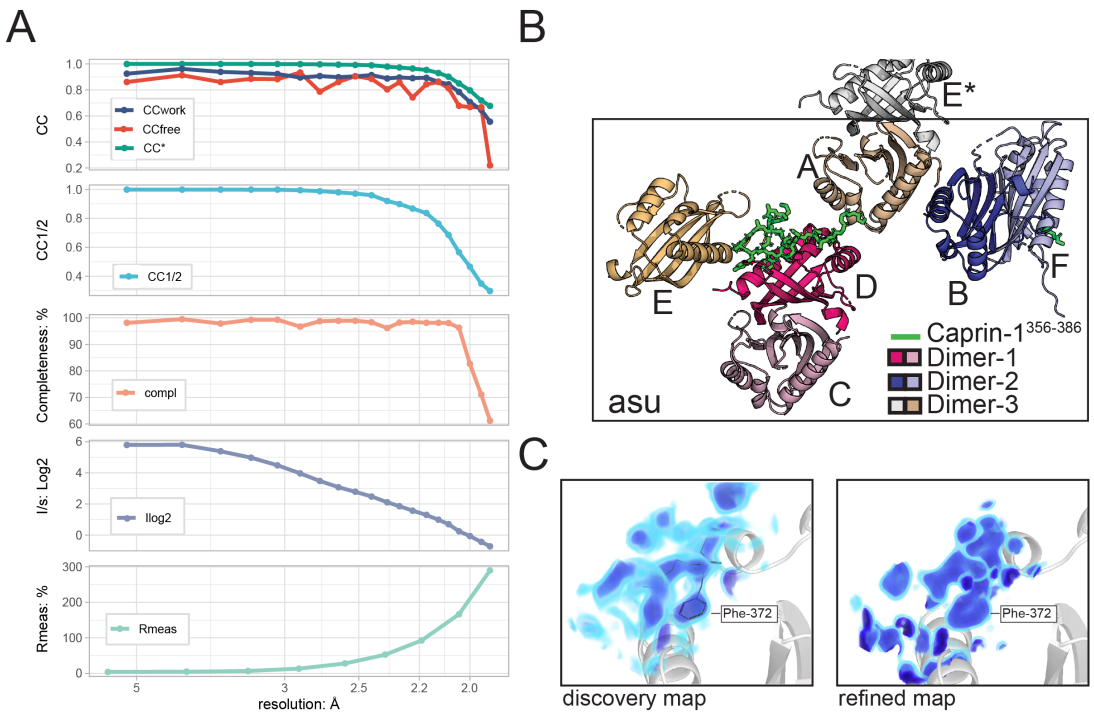

Figure S1. Crystallographic quality indicators and asymmetric unit of PDB structure 6TA7. *Related to Figure 1.*

(A) Crystallographic quality indicators [1–5] were plotted against resolution shells: *CC1/2:* CC between intensity estimates from half data sets; *CCstar:* Calculated from CC1/2. Indicator useful for comparing data and model quality. *CCwork and CCfree:* the standard and cross validated correlations of the experimental intensities, with the intensities calculated from the refined molecular model. *I/σ*: Average signal-to-noise ratio of individual observations, given on log2-scale. Data fall below I/ σ < 2 at a resolution of about 2.1 Å. *Rmeas:* Multiplicity independent replacement of Rmerge and Rsym; Useful for assessing space group symmetry and isomorphism of multiple data sets; Should play no role in determining resolution cutoff. *Completeness:* Percentage of measured unique reflections out of the expected ones. Additional crystallographic statistics typically are listed in Table S1.

(B) The asymmetric unit of the G3BP1-NTF2/ Caprin-1$^{356-386}$ crystal structure contains three non-identical NTF2-dimers created by chains C/D, A/E and B/F. The 20AA-long and 4AA-short Caprin-1 fragments bound to NTF2 chains D and F, respectively.

(C) The discovery and refined maps as well as the built model of Phe-372 and few additional backbone atoms of the shorter Caprin-1$^{356-386}$ fragment are visualized similarly to Figure 1B.

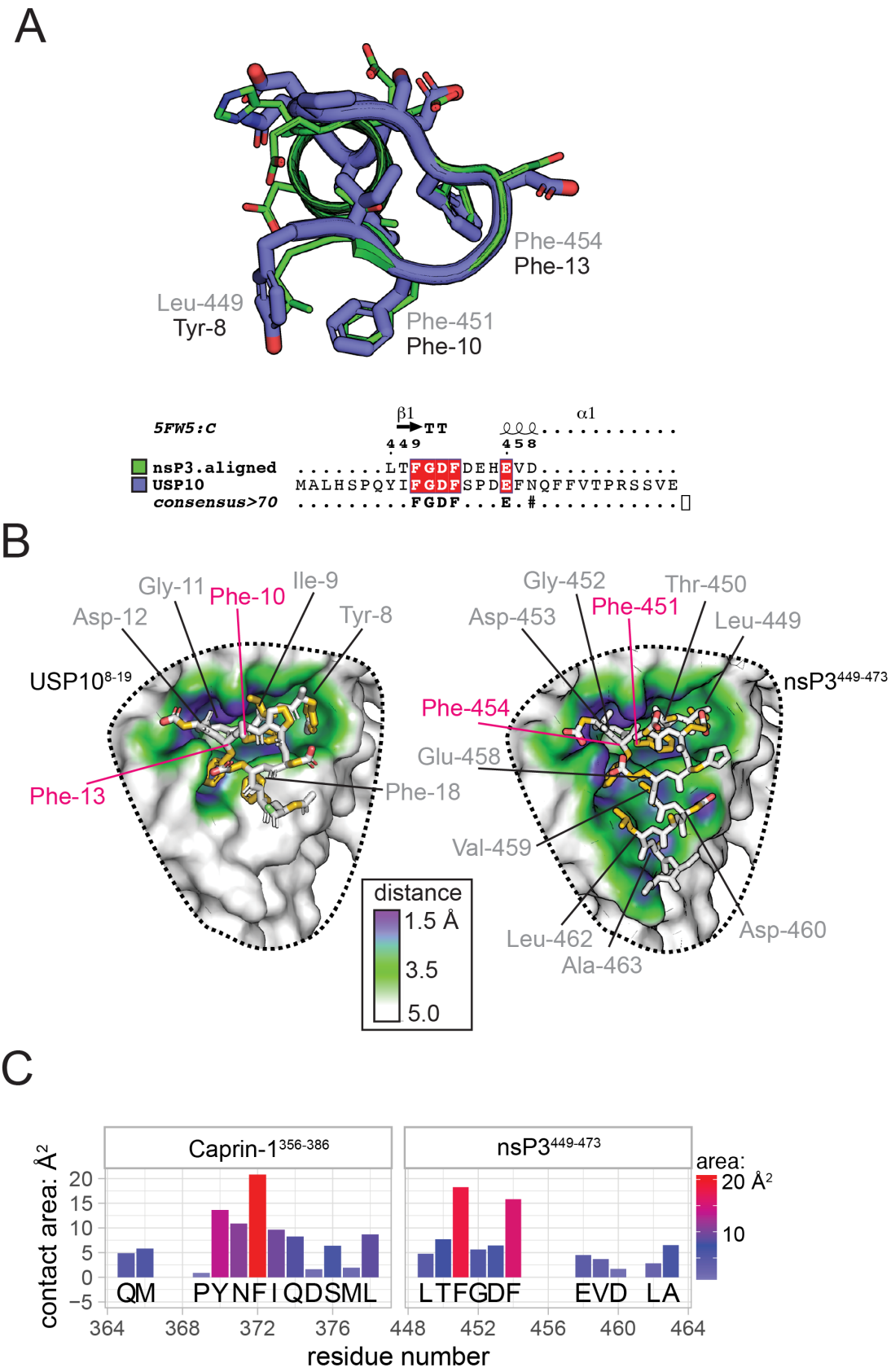

Figure S2. Molecular model for USP10$^{8-19}$ binding to NTF2 and nsP3 contact interface areas. *Related to Figures 1 and 3.*

(A) The structure of USP10$^{8\text{-}19}$ was predicted based on nsP3$^{449–473}$ as a template using Phyre, and manually adapted in Coot to include Tyr-8 that was not modeled and then refined using Rosetta FlexPepDock. The aligned sequence was visualized using ESPript [6–8].

(B) The putative binding interface of the docked USP10 was visualized similarly to Figure 3.

(C) Residue-level contact interface areas integrated from the Molprobity output tables highlighted key aromatic anchors of Caprin-1 and nsP3, as well as contact hot spots.

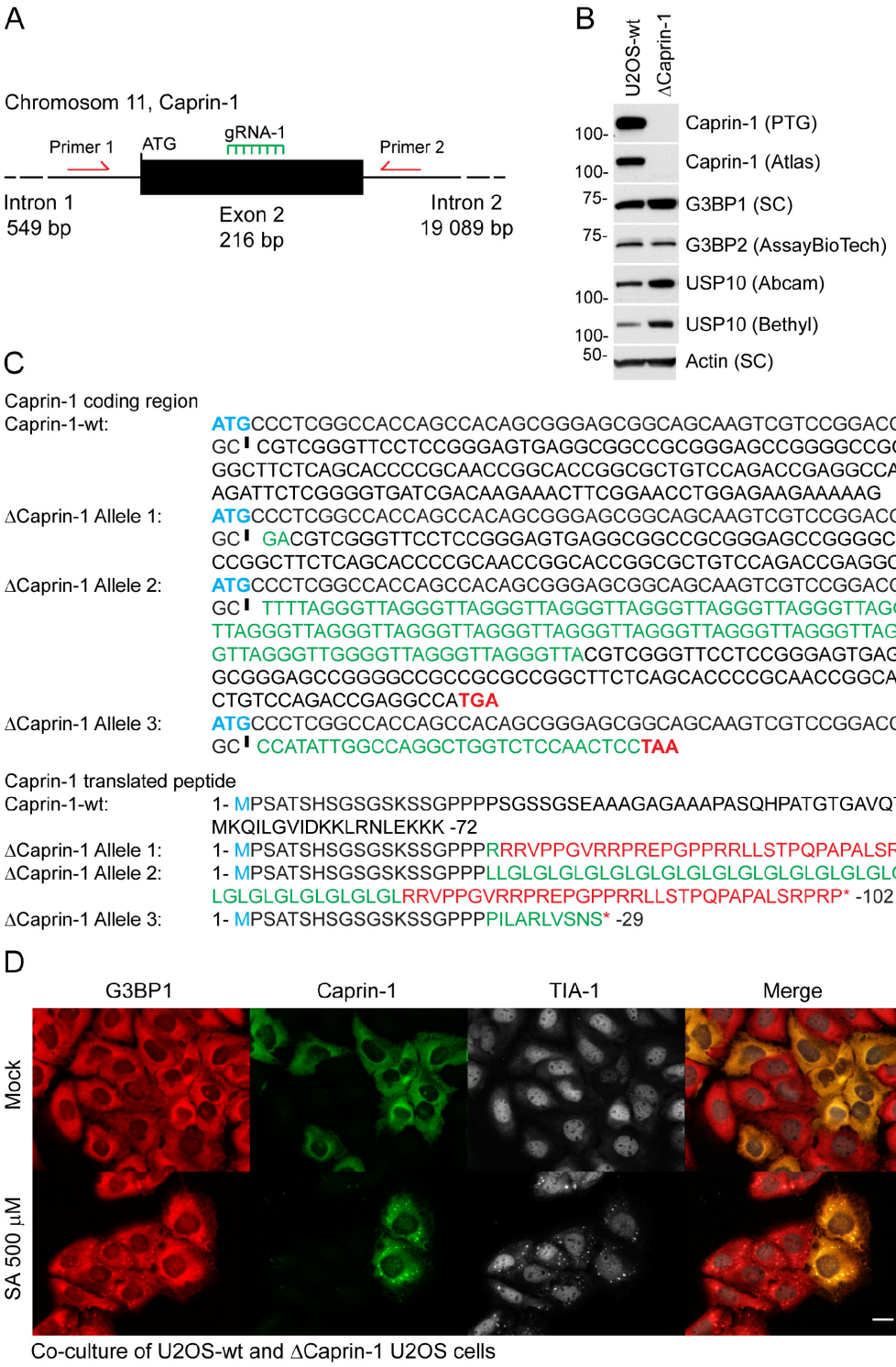

Co-culture of U2OS-wt and ΔCaprin-1 U2OS cells

Figure S3. Creation and evaluation of U2OS Caprin-1 knockout cells using CRISPR/Cas9 technology. *Related to Figures 2 and 7.*

(A) CRISPR/Cas9 mediated deletion of Caprin-1 utilizing guide RNA located within the second exon of Caprin-1. Green line indicates location of gRNA and red arrows denote primers used for genotyping and sequencing.

(B) Western blotting confirms loss of Caprin-1 expression with two different commercial antibodies, while direct interaction partners G3BP1 and G3BP2 are unaffected, interaction competitor USP10 is upregulated. Actin serves as loading control.

(C) Genotype of U2OS ΔCaprin-1 cells. Gene sequences showing Cas9-induced insertions (green); initiator ATG appears bold blue, black vertical line indicates Cas9 double-strand break, inframe premature stop appears in bold red. Predicted translated peptides of native gene are aligned above the three mutant alleles, with predicted frameshifted aa (Blue start methionine, black native aa; green inserted aa and red frameshifted native aa) and premature stop codons (red asterisks).

(D) U2OS-WT and U2OS ΔCaprin-1 cells, co-cultured, treated as indicated and stained for G3BP1 (red), Caprin-1 (green), and TIA-1 (grey). Scale bar is 20 μm.

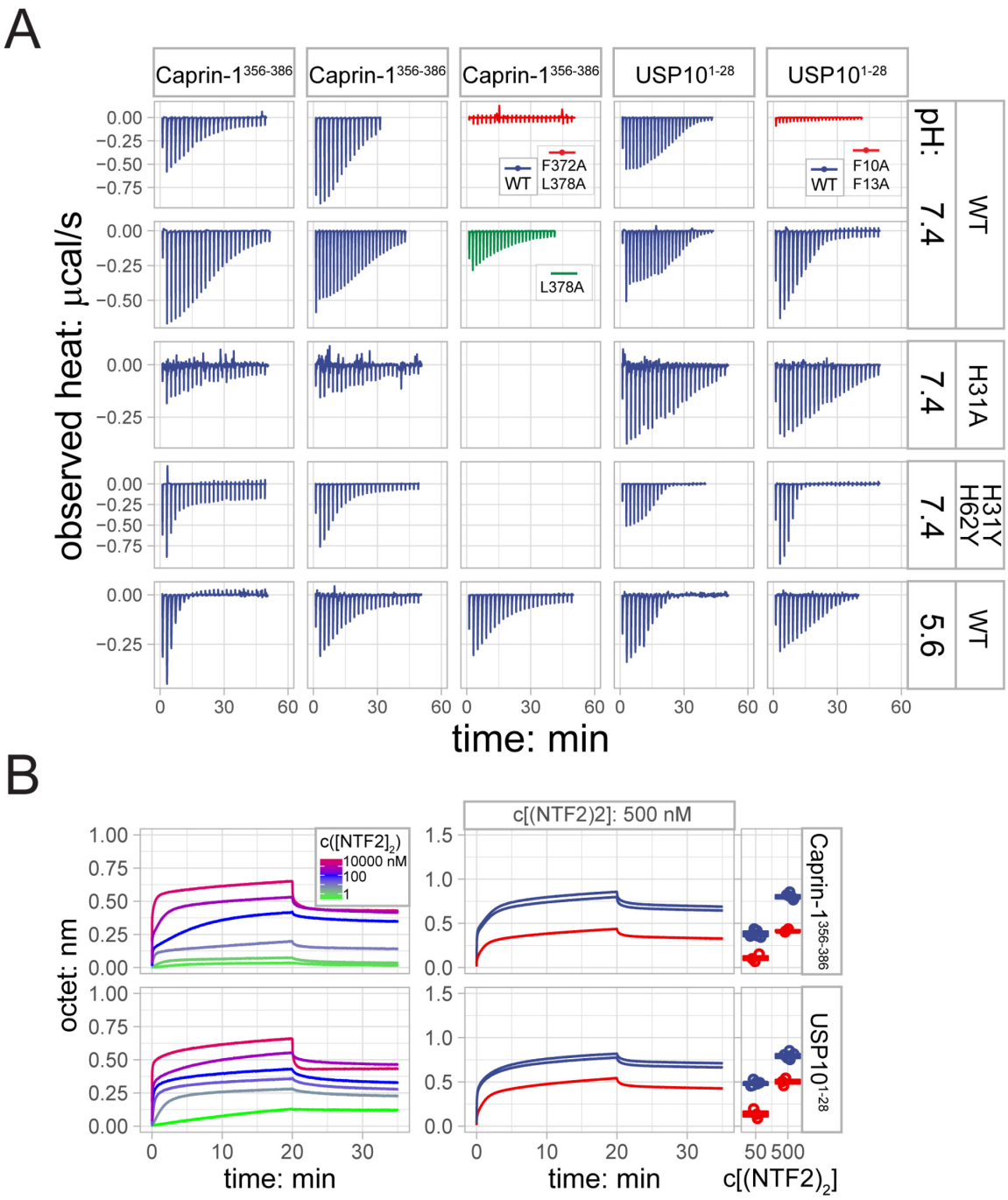

53 **Figure S4. ITC thermograms and BLI kinetic traces.** *Related to Figures 2 and 4.*

54 (A) Baseline-corrected thermograms from which the integrated binding heats were derived.
55 Thermograms are colored as in Figure 2. The measurement group comprising NTF2-wildtype
56 and NTF2-H31YH62Y at pH 7.4 were performed at approximately double active
57 concentrations compared to the other two measurement groups, as apparent from the double-
58 scaled raw data. The K_D and ΔH values obtained from the global heterogeneous 1:1 model fits
59 to the derived binding isotherms are summarized in Table S2.

(B) In BLI binding of the NTF2 dimer ($NTF2_2$) to surface-immobilized GFP-$USP10^{1-28}$ and GFP-$Caprin^{356-386}$ yielded very fast association and very slow dissociation phases for both interactions, most likely due to electrostatic attraction of NTF2 to the sensor surface and the bivalent nature of the analyte. Pseudo-equilibrium binding levels were derived from the final timepoints of the association phases of each titration. *left panel* Representative curves from in total 32 and 40 curves for GFP-$Caprin^{356-386}$ and GFP-$USP10^{1-28}$. *middle panel*: Kinetic binding curves measured at NTF2-concentration of 500 nM. *right panel:* Boxplots of binding response levels at NTF2-concentrations of 50 and 500 nM from three measurement repeats of each set. Binding levels of 500 nM NTF2 to the double mutants (red line) reached approximately the binding levels of WT NTF2 at 50 nM, indicating that binding of NTF2 to the mutants was estimated to be about ten times weaker.

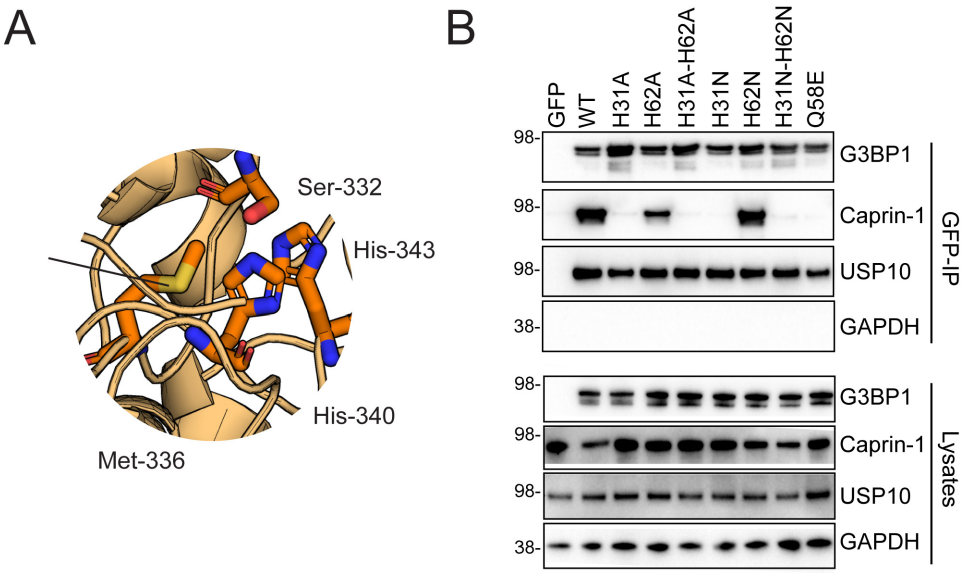

Figure S5. pH-sensitive polymerization site of fibrinogen and co-IP of GFP-G3BP1:Caprin-1 . *Related to Figure 4.*

(A) A similar three dimensional arrangement as for G3BP1:Caprin-1 site 3 was identified in the pH-sensitive polymerization site of fibrinogen comprising His-340, His-343, Met-336 and Ser-332.

(B) U2OS ΔΔG3BP1/2 cells were stably transfected with indicated GFP-G3BP1 mutant constructs. GFP immunoprecipitates and full cell lysates were analyzed by Western blot for G3BP1, Caprin-1, USP10 or GAPDH. Data are representative of at least five repeated experiments.

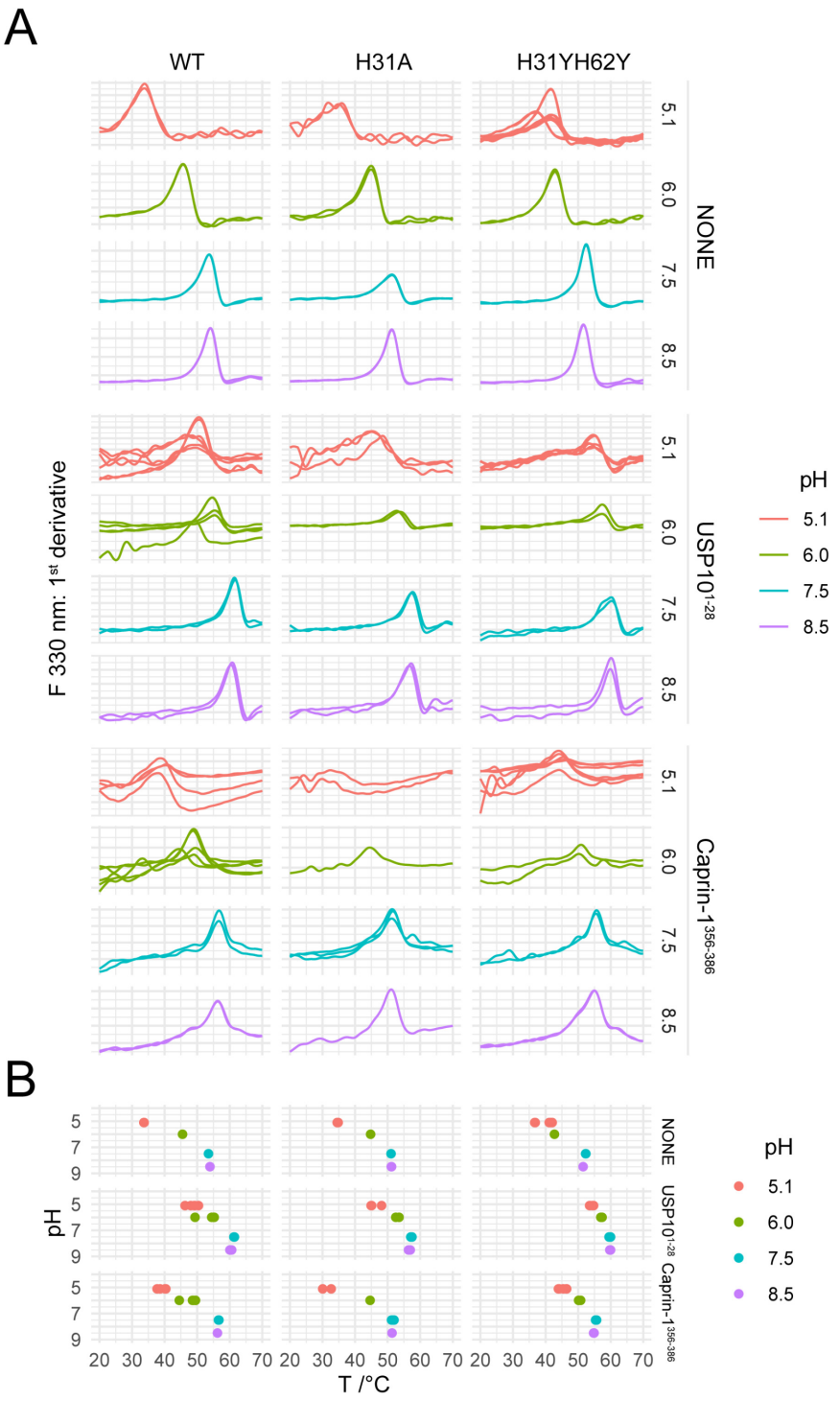

Figure S6. nanoDSF data. *Related to Figure 4.*

(A) In thermal unfolding experiments using the Prometheus nanoDSF system, protein samples are heated at a constant rate and thermal melting is monitored as a change in fluorescence of intrinsic aromatic residues at high resolution (https://nanotempertech.com/), revealing midpoint transition temperatures (T_m) as first derivative peak maxima. The first derivative of the fluorescence recorded at 330 nm is shown in panel columns and rows for the G3BP1-NTF2 construct and the ligands at the tested pH, respectively.

(B) The derived T_m-values (peak maximum) of each curve are plotted versus pH in panel columns and rows for the G3BP1-NTF2 construct and the ligands, respectively.

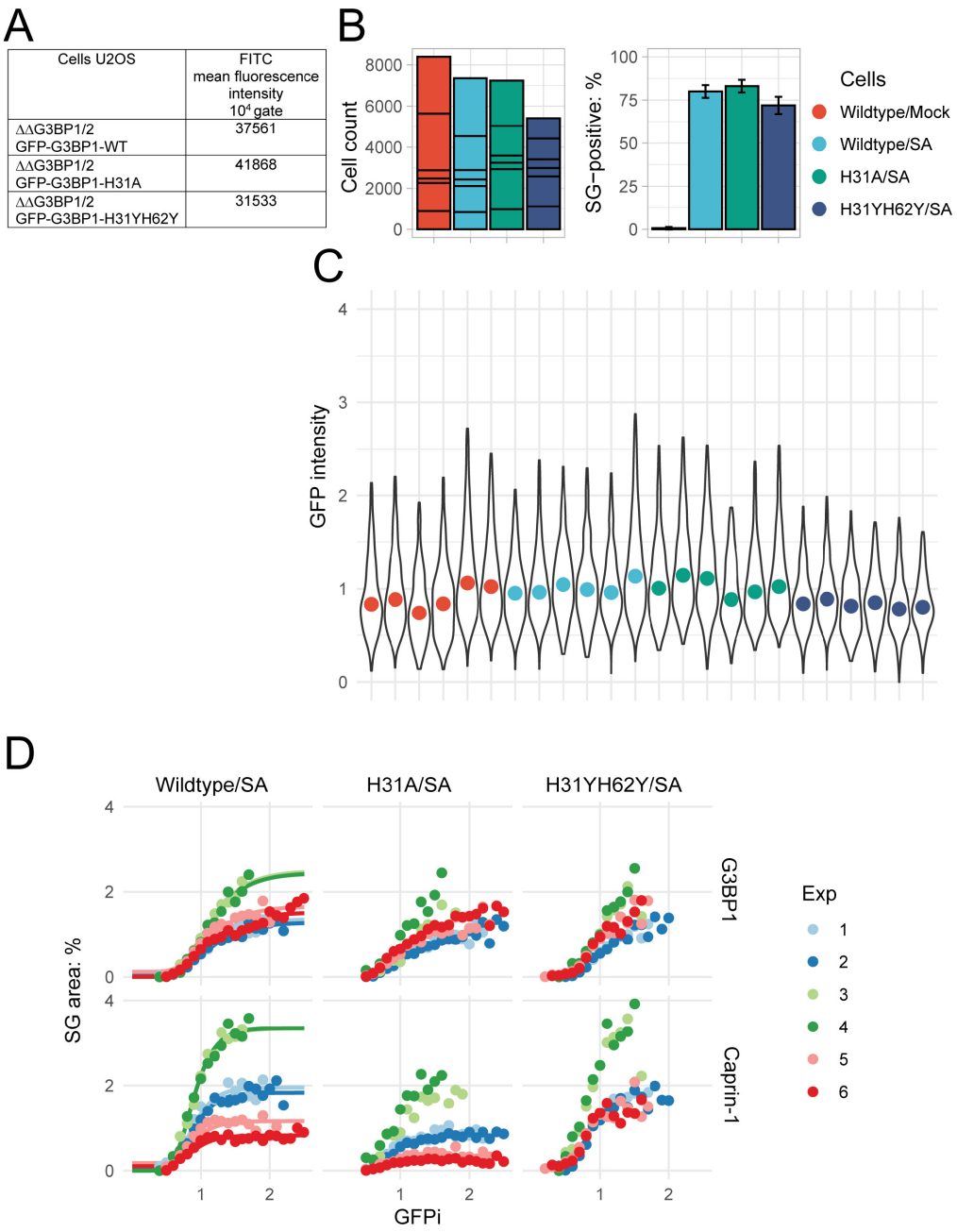

90 **Figure S7. High content microscopy analysis of presorted U2OS ΔΔG3BP1/2 cells stably**
91 **expressing G3BP1-WT, -H31A and -H31YH62Y.** *Related to Figure 5.*

92 (A) FACS sort and comparison. Frequencies of GFP-G3BP1-WT, H31A and H31YH62Y
93 cells are plotted against GFP intensities (FITC channel).

94 (B) Total counts of GFP-positive cells per experiment yielded total numbers between 5000
95 and 8000 cells. The percentages of GFP-G3BP1 SG-positive cells of each population were
96 determined separately for each experiment (n = 6), combined and visualized as a bar chart.
97 Data shown are mean ± SEM.

(C) The distribution of cellular mean GFP intensity values are visualized as violin plots for each cell population and single experiment. Median values are highlighted and colored as in panel B.

(D) Stress granule area is plotted against the median GFP-intensity value of each cell population grouped into intensity bins for every single experiment and separately for the GFP and Caprin-1 channels.

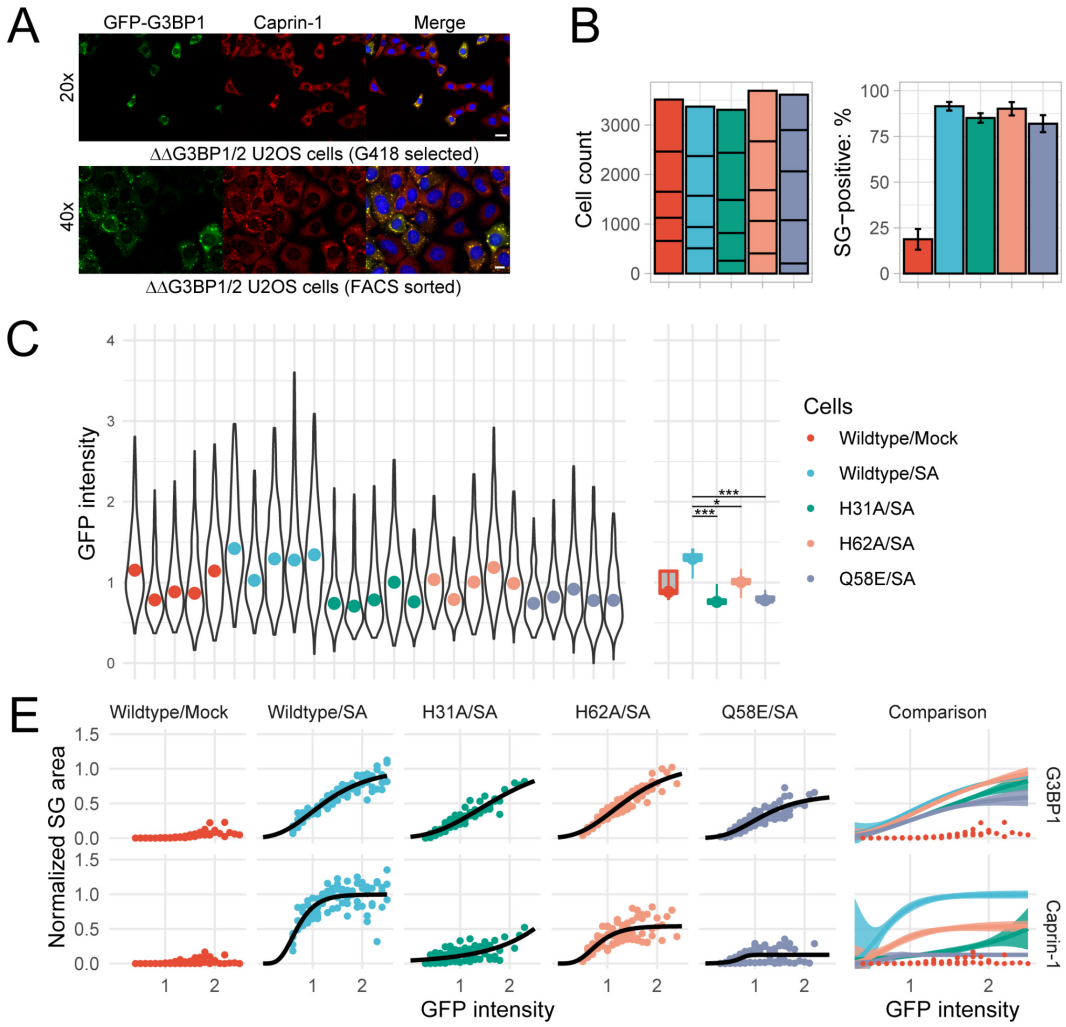

Figure S8. Additional high-content microscopy dataset of U2OS ΔΔG3BP1/2 cells stably expressing G3BP1-WT, -H31A, -H62A and –Q58E. *Related to Figure 5.*

(A) Representative high-content microscopy images of G418 drug selected (upper panel) and FACS sorted (lower panel) U2OS ΔΔG3BP1/2 cells expressing GFP-G3BP1-WT (green) were stressed with sodium arsenite (200 µM) for 1h, stained for endogenous Caprin-1 (red) and nuclei (Hoechst, blue). Magnification 20x, bar 40 µm (upper panel) Magnification 40x, bar 20 µm (lower panel).

(B) Total counts of GFP-positive cells per experiment yielded numbers of around 3000 cells for each population. The percentages of GFP-G3BP1 SG-positive cells of each population were determined separately for each experiment (n = 5), combined and visualized as a bar chart. Data shown are mean ± SEM.

(C) Left panel. Distribution of cellular median GFP intensity values are visualized as violin plots for each cell population and single experiment. Right panel. Intensities of GFP-G3BP1 cells of each population were determined separately for each experiment (n = 5) as shown in

right panel, combined and visualized as a boxplot. Significance p-levels were obtained from post-hoc ANOVA Tukey HSD: *_≤ 0.05, ** ≤ 0.01, *** ≤ 0.001. The significance labels for the comparison between stressed and unstressed mock cells were removed.

(E) The normalized SG area is plotted against the median GFP-intensity value of cells grouped into intensity bins in each experiment. SG areas were normalized to the maximal SG area of G3BP1-WT, separately for the GFP and Caprin-1 channels. Right panel: Comparison of dose-response curves from left panel with added 95% confidence intervals.

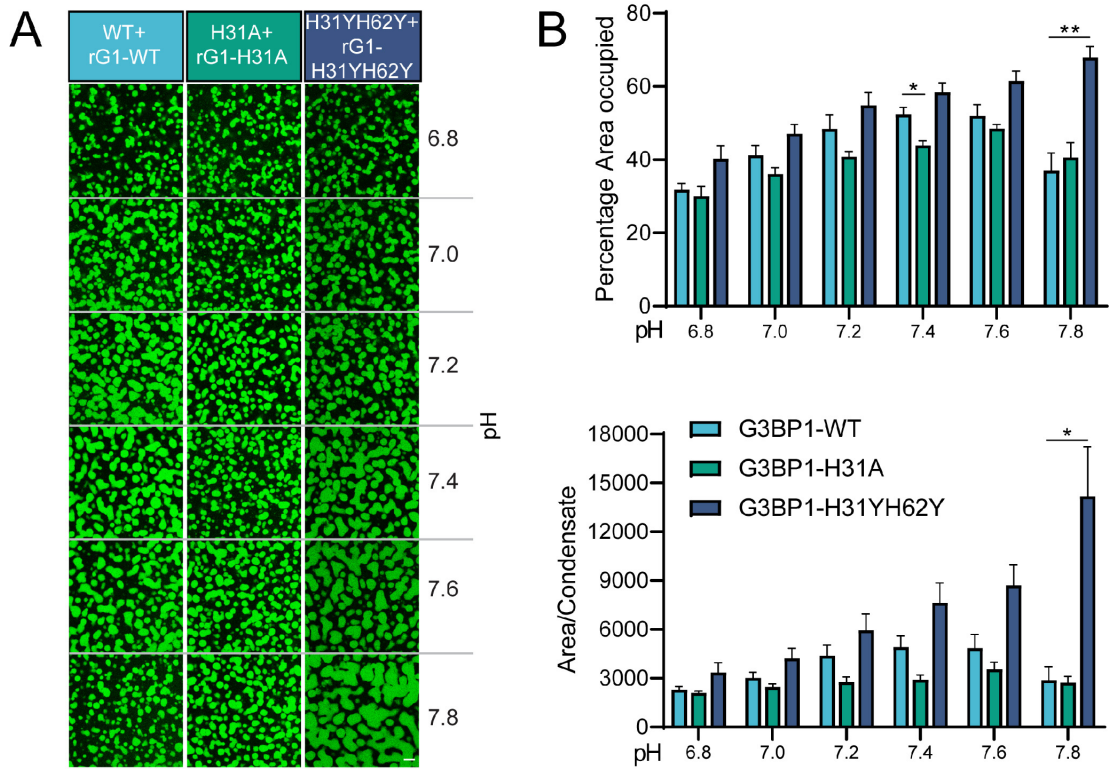

126

127 **Figure S9. Dysregulated condensate formation in H31A and H31YH62Y mutants at**
128 **various pH levels.** *Related to Figure 5.*

129 (A) Addition of 20 µM recombinant G3BP1-WT, -H31A, -H31Y-H62Y to pH adjusted cell
130 lysates from U2OS ΔΔG3BP1/2 cells stably expressing G3BP1-WT, -H31A and -H31YH62Y
131 induces condensates. Images were taken 60 min following formation of condensates. Bar 10
132 µm.

133 (B) Quantification of condensates by percentage of area occupied and by area per condensate.
134 Data shown are mean ± SEM and are analyzed using an unpaired t test. * $P < 0.05$, ** $P <$
135 0.01; n = 3.

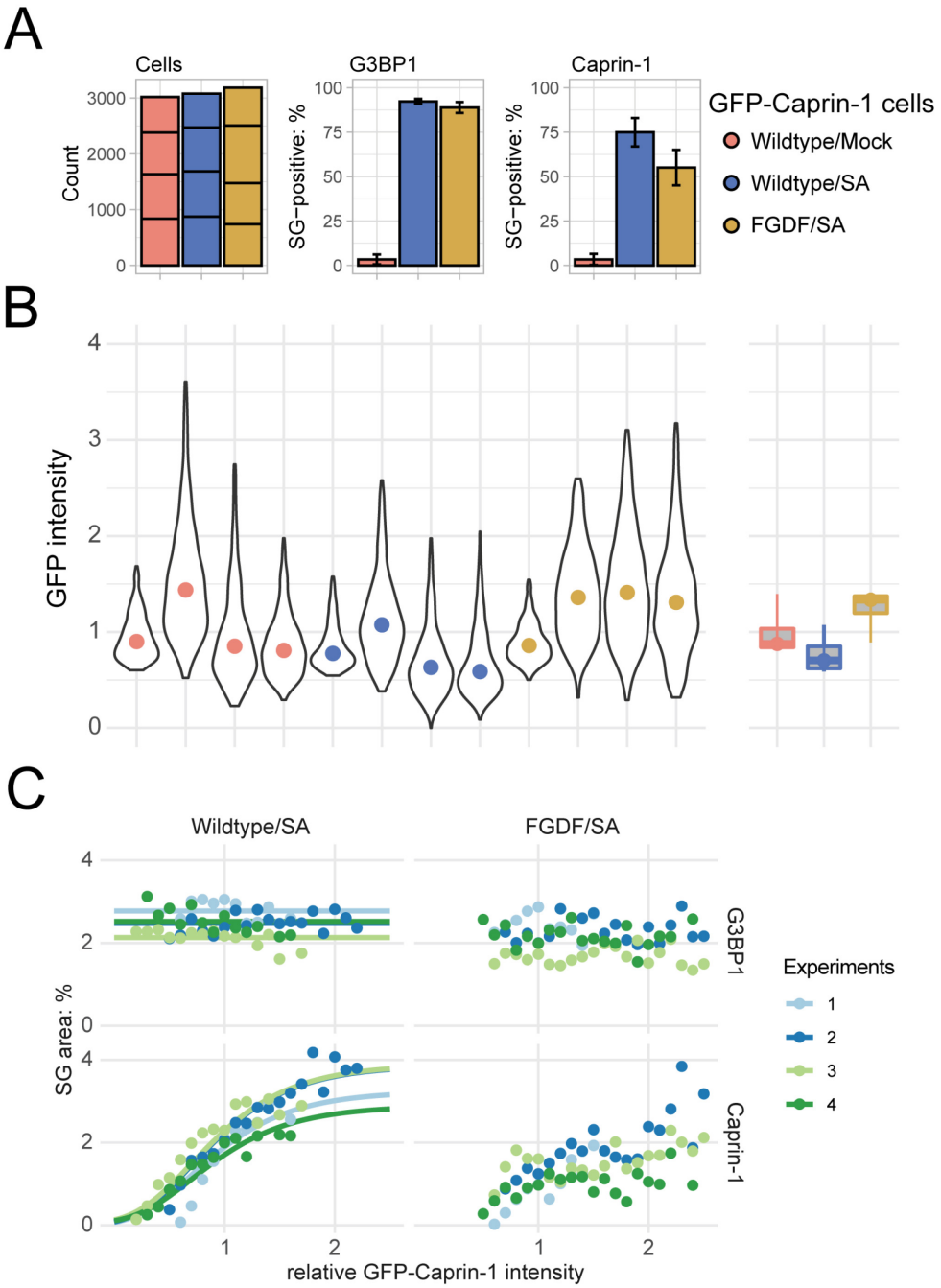

Figure S10. High content microscopy of U2OS ΔCaprin-1 cells stably expressing GFP-Caprin-1-WT or GFP-Caprin-1-FGDF. *Related to Figure 7.*

(A) Total counts of GFP-positive cells per experiment yielded numbers of around 3000 cells for each population (left panel). The percentages of GFP-G3BP1 SG-positive (middle panel) and Caprin-1 SG positive cells (right panel) of each population were determined separately for each experiment (n = 4), combined and visualized as a bar chart. Data shown are mean ± SEM.

(B) The distribution of cellular GFP intensities are visualized as violin plots for each cell population and single experiment and combined in the right panel.

(C) Stress granule area is plotted against the median GFP-intensity value of each cell population grouped into intensity bins for every single experiment separately for the G3BP1 and GFP-Caprin-1 channels.

Supplemental lists and tables.

List S1. Protein constructs used for crystallization and biophysical measurements

>His6-TEV-G3BP1-***NTF2***

MHHHHHHSSGVDLGT*ENLYFQ*-

SMVMEKPSPLLVGREFVRQYYTLLNQAPDMLHRFYGKNSSYVHGGLDSNGKPADAVYGQKEIHRKVM SQNFTNCHTKIRHVDAHATLNDGVVVQVMGLLSNNNQALRRFMQTFVLAPEGSVANKFYVHNDIFRY QDEVFG

>twSTII-TEV-GFP-USP10$^{1\text{-}28}$ / -F3AF6A // -Caprin-1$^{356\text{-}386}$ / -F3AL9A

MSAWSHPQFEKGGGSGGGSGSAWSHPQFEKSGG*ENLYFQ-*

*G*GGSVSKGEELFTGVVPILVELDGDVNGHKFSVSGEGEGDATYGKLTLKFICTTGKLPVPWPTLVTTLT YGVQCFSRYPDHMKQHDFFKSAMPEGYVQERTIFFKDDGNYKTRAEVKFEGDTLVNRIELKGIDFKED GNILGHKLEYNYNSHNVYIMADKQKNGIKVNFKIRHNIEDGSVQLADHYQQNTPIGDGPVLLPDNHYL STQSALSKDPNEKRDHMVLLEFVTAAGITLGMDELYKSENQG-

MALHSPQYIFGDFSPDEFNQFFVTPRSS

… MALHSPQYIAGDASPDEFNQFFVTPRSS

… RQRVQDLMAQMQGPYNFIQDSMLDFENQTLD

… RQRVQDLMAQMQGPYNAIQDSMADFENQTLD

We used the primer design tool (https://joschif.github.io/SLIC/) for SLIC-based cloning

Table S1. Crystallographic data table of PDB:6TA7

Resolution range	46.5 - 1.93 (2.00 - 1.93)
Space group	P 21 21 21
Unit cell	81.6 100 113.3 / 90 90 90
Total reflections	898968 (58966)
Unique reflections	66520 (4630)
Multiplicity	13.5 (12.7)
Completeness (%)	94 (66)
Mean I/sigma(I)	14.6 (0.7)
Wilson B-factor	40
R-meas	0.12 (3.4)
CC1/2	1 (0.33)
CC*	1 (0.70)
Reflections used in refinement	66502 (4630)
Reflections used for R-free	2098 (146)
R-work	0.21 (0.38)
R-free	0.25 (0.43)
CC(work)	0.96 (0.61)
CC(free)	0.92 (0.51)
Number of non-hydrogen atoms	6524
number_macromol	6246

number_ligands	3
Protein residues	792
RMS(bonds)	0.007
RMS(angles)	0.78
Ramachandran allowed (%)	99.8
Ramachandran favored (%)	97
Rotamer outliers (%)	1.2
Clashscore	5.28
Average B-factor (ADP)	61
ADP macromolecules	61
ADP ligands	54
ADP solvent	55

Table S2. K_D and ΔH values from the global 1:1 model fits to ITC binding isotherms

		WT pH 7.4	H31A pH 7.4	H31YH62Y pH 7.4	WT pH 5.6
K_D [μM]	$USP10^{1-28}$	1.0 ± 0.2	2.6 ± 0.7	0.5 ± 0.3	0.4 ± 0.3
	$Caprin^{356-386}$	2.2 ± 0.4	14 ± 11	2.1 ± 0.4	1.4 ± 1.0
ΔH [kcal/mol]	$USP10^{1-28}$	-15.5 ± 0.4	-16.3 ± 0.8	-13.7 ± 0.9	-17.6 ± 1.7
	$Caprin^{356-386}$	-16.4 ± 0.4	-11.9 ± 3.0	-19.3 ± 0.8	-13.7 ± 2.3

Table S3. CRISPR/Cas9 sequence list

CRISPR/Cas9 KO	gDNA	Sequence
Caprin-1	g1	5′-GTCCGGACCGCCACCGCCGT- 3′

	g2	5′-CTCCCGGAGGAACCCGACGG- 3′

174

175 **Table S4 Primer list**

Plasmid	Forward primer 5′ phosphorylated	Reverse primer 5′ phosphorylated
Exo-2 Caprin-1 amplification	5′gccccgtccgtctcctg 3’	5’ aggaggggacctagtaacgctc 3’
pEGFP-C1-G3BP1-H31A	5′cccagacatgctgGCAagattttatggaaag-3′	5′gcctggttcagcagtgtgtaatactg-3′
pEGFP-C1-G3BP1-H31N	5′cccagacatgctgAACagattttatggaaag-3′	′gcctggttcagcagtgtgtaatactg-3′
pEGFP-C1-G3BP1-H31Y	Primer for Gibson cloning Template: pEGFP-C1-G3BP1-WT Insert: 5′ctgaaccaggccccagacatgctgTACagattttatggaaagaac-3′ Backbone: 5′cagcatgtctggggcctggttcagcagtgtgtaatactgtc-3′	Insert 5′gtaccgtcgactgcagaattcttactgccgtggcgcaagc-3′ Backbone: 5′gaattctgcagtcgacggtaccgcgggcccgggatccacc-3′
pEGFP-C1-G3BP1-Q58E	5′ccagcagatgcagtctacggaGAGaaagaaatcc-3′	5′ctttccatttgaatccaatcccccatgga-3′
pEGFP-C1-G3BP1-H62A	5′ggacagaaagaaatcGCAaggaaagtgatg-3′	5′gtagactgcatctgctggctttcc-3′
pEGFP-C1-G3BP1-H62N	5′ggacagaaagaaatcAACaggaaagtgatg-3′	5′gtagactgcatctgctggctttcc-3′
pEGFP-C1-G3BP1-H31A-H62A	Template: pEGFP-C1-G3BP1-H31A 5′ggacagaaagaaatcGCAaggaaagtgatg-3′	5′gtagactgcatctgctggctttcc-3′
pEGFP-C1-G3BP1-H31N-H62N	Template: pEGFP-C1-G3BP1-H31N 5′ggacagaaagaaatcAACaggaaagtgatg-3′	5′gtagactgcatctgctggctttcc-3′
pEGFP-C1-G3BP1-H31Y-H62Y	Primer for Gibson cloning Template: pEGFP-C1-G3BP1-H31Y Insert: 5′gtctacggacagaaagaaatcTACaggaaagtgatgtcac-3′ Backbone: 5′cagcatgtctggggcctggttcagcagtgtgtaatactgtc-3′	Insert: 5′gtaccgtcgactgcagaattCttactgccgtggcgcaagc-3′ Backbone: 5′gaattctgcagtcgacggtaccgcgggcccgggatccacc-3′
pAcGFP-C1-Caprin1-Q360A	5′agcgagtaGCAgaccttatggcacaaatg-3′	5′gtcttctcacaaggggatctgcc-3′
pAcGFP-C1-Caprin1-D361A	5′agcgagtacaaGCActtatggcacaaatg-3′	5′gtcttctcacaaggggatctgcc-3′

pAcGFP-C1-Caprin1-L362A	5′agcgagtacaagacGCAatggcacaaatg-3′	5′gtcttctcacaaggggatctgcc-3′
pAcGFP-C1-Caprin1-M363A	5′aagaccttGCAgcacaaatgcagggtcc-3′	5′gtactcgctgtcttctcacaaggg-3′
pAcGFP-C1-Caprin1-Q365A	5′aagaccttatggcaGCAatgcagggtcc-3′	5′gtactcgctgtcttctcacaaggg-3′
pAcGFP-C1-Caprin1-M366A	5′ttatggcacaaGCAcagggtccctataatttcatac-3′	5′ggtcttgtactcgctgtcttctcac-3′
pAcGFP-C1-Caprin1-Q367A	5′cttatggcacaaatgGCAggtccctataatttcatac-3′	5′gtcttgtactcgctgtcttctcacaagg-3′
pAcGFP-C1-Caprin1-G368A	5′cttatggcacaaatgcagGCAccctataatttcatac-3′	5′gtcttgtactcgctgtcttctcacaagg-3′
pAcGFP-C1-Caprin1-P369A	5′ttatggcacaaatgcagggtGCAtataatttcatac-3′	5′ggtcttgtactcgctgtcttctcac-3′
pAcGFP-C1-Caprin1-Y370A	5′cagggtcccGCAaatttcatacaggattcaatgctg-3′	5′catttgtgccataaggtcttgtactcgc-3′
pAcGFP-C1-Caprin1-N371A	5′cagggtccctatGCAttcatacaggattcaatgctg-3′	5′catttgtgccataaggtcttgtactcgc-3′
pAcGFP-C1-Caprin1-F372A	5′cagggtccctataatGCAatacaggattcaatgctg-3′	5′catttgtgccataaggtcttgtactcgc-3′
pAcGFP-C1-Caprin1-I373A	5′cagggtccctataatttcGCAcaggattcaatgctg-3′	5′catttgtgccataaggtcttgtactcgc-3′
pAcGFP-C1-Caprin1-Q374A	5′cagggtccctataatttcataGCAgattcaatgctg-3′	5′catttgtgccataaggtcttgtactcgc-3′
pAcGFP-C1-Caprin1-D375A	5′cctataatttcatacagGCAtcaatgctggattttg-3′	5′gaccctgcatttgtgccataagg-3′
pAcGFP-C1-Caprin1-S376A	5′tttcatacaggatGCAatgctggattttgaaaatcag-3′	5′ttatagggaccctgcatttgtgccataag-3′
pAcGFP-C1-Caprin1-M377A	5′tttcatacaggattcaGCActggattttgaaaatcag-3′	5′ttatagggaccctgcatttgtgccataag-3′
pAcGFP-C1-Caprin1-L378A	5′ggattcaatgGCTgattttgaaaatcagacactt-3′	5′tgtatgaaattatagggaccctgcatttgtgc-3′
pAcGFP-C1-Caprin1-D379A	5′ggattcaatgctgGCTtttgaaaatcagacactt-3′	5′tgtatgaaattatagggaccctgcatttgtgc-3′
pAcGFP-C1-Caprin1-F380A	5′ggattcaatgctggatGCTgaaaatcagacactt-3′	5′tgtatgaaattatagggaccctgcatttgtgc-3′
pAcGFP-C1-Caprin1-E381A	5′ggattcaatgctggattttGCTaatcagacactt-3′	5′tgtatgaaattatagggaccctgcatttgtgc-3′
pAC-GFP-Caprin-1-chimera	Template Backbone: pAcGFP-C1-Caprin1-WT 5’atcaattctttgtgactcctacacttgatcctgccattgt-3 Template Insert: pAcGFP-C1-USP10-1-40-WT 5’ttgtgagaagacagcgagtaatggccctccacagcccgca-3’	Template Backbone: pAcGFP-C1-Caprin1-WT 5’tgcgggctgtggagggccattactcgctgtcttctcacaa-3’ Template Insert: pAcGFP-C1-USP10-1-40-WT 5’acaatggcaggatcaagtgtaggagtcacaaagaattgat-3’

176

177 **Table S5 Antibody list**

Antigen	Species	Catalog number	Source	RRIDs
Actin	Mouse	Sc-8432	Santa Cruz Biotechnology, Inc.	AB_626630
Caprin-1	Rabbit	15112-1-AP	Proteintech group	AB_2070016
Caprin-1	Rabbit	HPA018126	Sigma-Aldrich	AB_1849929
FMR1	Rabbit	13755-1-AP	Proteintech group	AB_2262872
GAPDH	Mouse	Sc-47724	Santa Cruz Biotechnology, Inc.	AB_627678
G3BP1	Mouse	Sc-365338	Santa Cruz Biotechnology, Inc.	AB_10846950
G3BP2	Rabbit	C18193	Assay Biotechnology	AB_10684426
TIA-1	Goat	Sc-1751	Santa Cruz Biotechnology, Inc.	AB_2201433
USP10	Rabbit	A300-900A	Bethyl Laboratories	AB_625312
USP10	Mouse	ab119418	Abcam	AB_10902427

178 **References**

179 1. Adams PD *et al.* 2002 PHENIX: building new software for automated crystallographic
180 structure determination. *Acta Crystallogr. D Biol. Crystallogr.* **58**, 1948–1954.

181 2. Kabsch W. 1993 Automatic processing of rotation diffraction data from crystals of initially
182 unknown symmetry and cell constants. *J. Appl. Crystallogr.* **26**, 795—800.
183 (doi:10.1107/S0021889893005588)

184 3. Karplus PA, Diederichs K. 2012 Linking crystallographic model and data quality. *Science*
185 **336**, 1030–1033. (doi:10.1126/science.1218231)

186 4. Karplus PA, Diederichs K. 2015 Assessing and maximizing data quality in
187 macromolecular crystallography. *Curr. Opin. Struct. Biol.* **34**, 60–68.
188 (doi:10.1016/j.sbi.2015.07.003)

189 5. Michael Krug MSW. 2012 XDSAPP: a graphical user interface for the convenient
190 processing of diffraction data using XDS. *J. Appl. Crystallogr.* **45**.
191 (doi:10.1107/S0021889812011715)

192 6. Gouet P, Courcelle E, Stuart DI, Métoz F. 1999 ESPript: analysis of multiple sequence
193 alignments in PostScript. *Bioinforma. Oxf. Engl.* **15**, 305–8.

194 7. Kelley LA, Sternberg MJE. 2009 Protein structure prediction on the Web: a case study
195 using the Phyre server. *Nat Protoc.* **4**, 363–371. (doi:10.1038/nprot.2009.2)

196 8. London N, Raveh B, Cohen E, Fathi G, Schueler-Furman O. 2011 Rosetta FlexPepDock
197 web server-high resolution modeling of peptide-protein interactions. *Nucleic Acids Res.*
198 **39**, W249–W253. (doi:10.1093/nar/gkr431)

199